Subduction initiation during collision-induced subduction transference: Numerical modeling and implications for the Tethyan evolution

Xinyi Zhong[1], Zhong-Hai Li[1*]

[1] Key Laboratory of Computational Geodynamics, College of Earth and Planetary Sciences, University of Chinese Academy of Sciences, Beijing 100049, China.

Corresponding author: Z.-H. Li (li.zhonghai@ucas.ac.cn)

Key Points:

- Forced convergence is required for the collision-induced subduction transference which generally occurs within 10 Myrs after collision.
- The weakness of passive margin significantly promotes subduction initiation after the terrane collision and accretion.
- The collision-induced subduction initiation of Neo-Tethyan plate may indicate large convergent force and/or weakened passive margin.

Abstract

The collision-induced subduction transference is a composite dynamic process including both the terrane collision/accretion and the subduction initiation (SI) at the neighboring passive margin. This process occurred repeatedly during the evolution of Tethyan systems, with multiple ribbon-like continents or micro-continents drifting from Gondwana in the southern hemisphere and accreting to the Eurasian continent since Paleozoic. In the previous numerical studies, the dynamics of terrane collision and induced SI are investigated individually, which however need to be integrated to study the controlling factors and time scales of collision-induced subduction transference. Systematic numerical models are conducted with variable properties of converging plates and different boundary conditions. The model results indicate that the forced convergence, rather than pure free subduction, is required to trigger and sustain the SI at the neighboring passive margin after terrane collision. In addition, a weak passive margin can significantly promote the occurrence of SI, by decreasing the required boundary force to reasonable value of plate tectonics. The lengths of subducted oceanic slab and accreting terrane play secondary roles in the occurrence of SI after collision. Under the favorable conditions of collision-induced subduction transference, the time required for SI after collision is generally short within 10 Myrs, which is consistent with the general geological records of Cimmerian collision and the following Neo-Tethyan SI. In contrast, the stable Indian passive margin and absence of SI in the present Indian Ocean may due to the low convergent force and/or the lack of proper weak zones, which remains an open question.

1 Introduction

In the plate tectonics and Wilson's cycle, the plate convergence starts with the subduction initiation (SI) and terminates with the continental collision and orogeny. Because of the low density of continental crust, the continental subduction-collision process cannot last for very long time as the oceanic subduction. Thereby, the plate convergence will generally stop after the orogeny with a timescale of several tens of million years, although the special case of India-Asia collision is still ongoing after ~50 Ma (*Yin and Harrison*, 2000; *Aitchison et al.*, 2007; *Najman, et al.*, 2010; *DeCelles et al.*, 2014; *Zhu et al.*, 2015). On the other hand, with the collision of a buoyant block, a new subduction zone may form in the neighboring plate to accommodate the continuous convergence, which is defined as the 'collision-induced subduction transference' (Figure 1a, b) *(Niu et al.*, 2003; *Stern*, 2004; *Zhu et al.*, 2011; *Stern and Gerya*, 2018). It may play a crucial role in the accretion and amalgamation of continents (*Stern*, 2017).

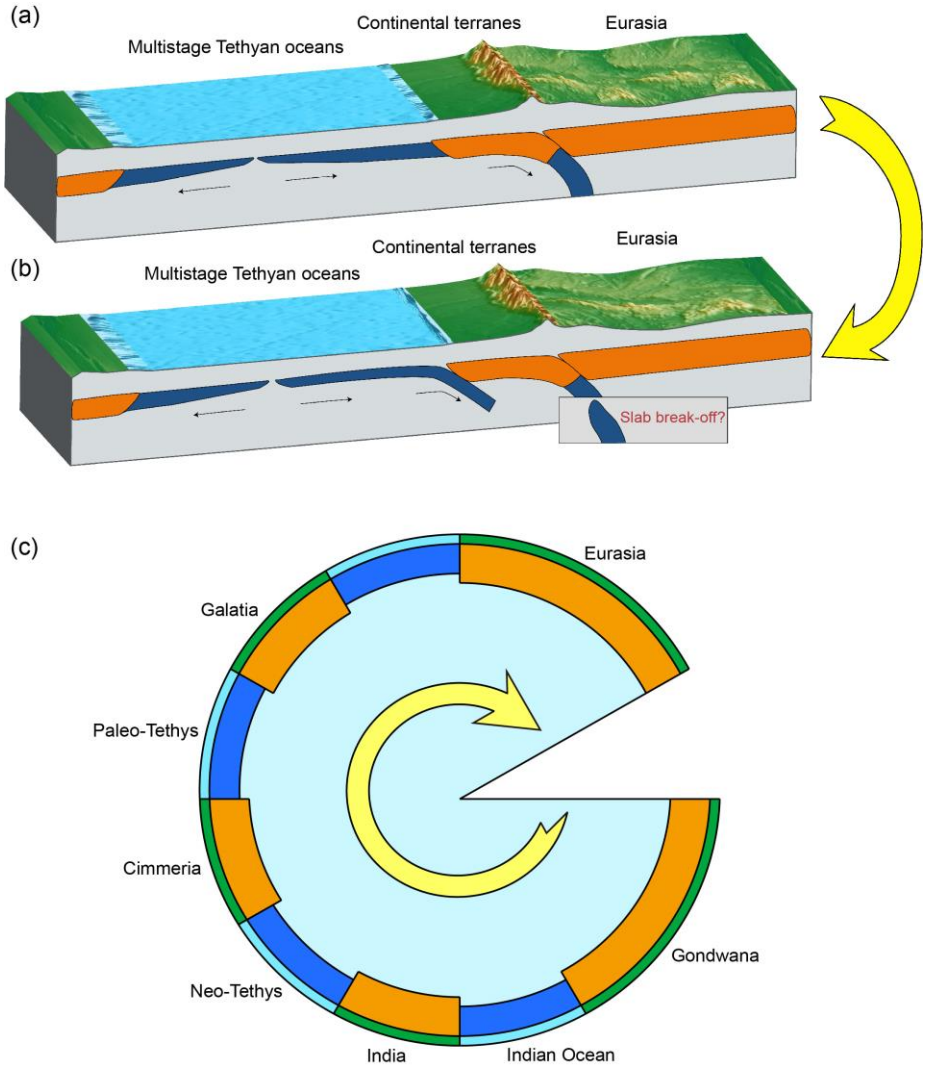

Figure 1. The conceptual sketch of repeated subduction initiation during collision-induced subduction transference and accretion of multiple continental terranes with Eurasian continent throughout the Tethyan evolution. **(a)** Collision of the continental terranes with Eurasia. **(b)**

Subduction initiation at the neighboring passive margin. **(c)** Multiple subduction-collision-subduction processes during the evolution of Tethyan system.

The collision-induced subduction transference, although without clear Cenozoic examples, is quite popular in the evolution of Tethyan system, which experienced multiple subduction-collision-subduction processes, as well as the assembly or accretion of terranes (Figure 1c) (*Şengör*, 1988; *Stampfli and Borel*, 2002; *Zhu et al.*, 2011, 2013; *Metcalfe*, 2013; *Wan et al.*, 2019). The ribbon-like continents or micro-continents continuously drifted from Gondwana in the southern hemisphere and accreted to the Eurasian continent throughout the evolution of the Tethyan system since Paleozoic (Figure 1c). The Tethyan system began with the breakup of the Galatian super terrane from the Gondwana, resulting in the opening of Paleo-Tethyan Ocean. The collision between the Galatian terrane and Laurasia finally closed the Rheic Ocean, with the subduction transferred to the Paleo-Tethys (*Stampfli* et al., 2013). Then, the Cimmerian terranes broke up from the Gondwana in late Paleozoic, leading to the opening of Neo-Tethyan Ocean. The collision of the Cimmerian terranes with Laurasia closed the Paleo-Tethys, after which the subduction was transferred to the Neo-Tethys in Mesozoic (*Stampfli and Borel*, 2002; *Zhu et al.*, 2013; *Wan et al.*, 2019). Finally, the Indian plate broke up from Gondwana in Cretaceous and collided with the Eurasian plate at around 55 Myrs (*Yin and Harrison*, 2000; *Aitchison et al.*, 2007; *Najman, et al.*, 2010; *DeCelles et al.*, 2014; *Zhu et al.*, 2015; *Searle*, 2019). Although the collision has lasted for a long time, there is still no clear sign for the SI in the present-day Indian Ocean (*Stern*, 2004; *Stern and Gerya*, 2018). Thus, it is still a mystery and challenge that whether and when the Indian Oceanic plate will begin subduction.

From the summarized Tethys evolution history, a crucial issue for the continuous plate convergence is the SI after the terrane collision and accretion, i.e. the collision-induced subduction transference (Figure 1a, b). Its dynamics is rarely investigated and thus still not resolved. The previous correlated numerical studies are generally focusing on two points. One is the subduction of anomalous blocks within an oceanic plate, including the island arc, oceanic plateaus or continental fragments, which is generally focusing on the resulting flat subduction (*van Hunen et al.*, 2002, 2004; *Mason et al.*, 2010) or the contrasting modes of accretion (e.g., *Selzer et al.*, 2008; *Tetreault and Buiter*, 2012; *Vogt and Gerya*, 2014; *Yang et al.*, 2018). Notably, a 'trench jump' after collision is predicted in some of the models (*Tetreault et al.*, 2012; *Vogt and Gerya*, 2014; *Yang et al.*, 2018), which is however caused by the detachment of weak and buoyant crust of the accreting terrane, rather than initiating a new subduction zone in the neighboring oceanic plate. Another type of model focuses on the SI at passive continental margins, which only deal with two plates and a transition between them (e.g., *Toth and Gurnis*, 1998; *Nikolaeva et al.*, 2011; *Rey et al.*, 2014; *Baes and Sobolev*, 2017; *Zhong and Li*, 2019; *Ulvrova et al.*, 2019). These models indicate that the SI at passive continental margin is not easy, which generally requires special conditions, for example, (1) the thin, weak and very buoyant continental lithosphere (e.g., *Nikolaeva et al.*, 2011; *Marques et al.*, 2013, 2014; *Rey et al.*, 2014), (2) a prescribed weak transition zone between the continental and oceanic plates (e.g. *Toth and Gurnis*, 1998; *Baes et al.*, 2011), (3) driven by downward mantle flow (e.g. *Baes and Sobolev*, 2017) or (4) driven by a boundary stress/force (e.g., *Zhong and Li*, 2019). On the other hand, the natural examples of Atlantic and Indian passive margins, neighboring to relatively old oceanic lithospheres, are generally stable and difficult for SI (*Cloetingh et al.*, 1989; *Mueller and Philips*, 1991, *Niu et al.*, 2003; *Stern and Gerya*, 2018; *Zhong and Li*, 2019). Thus, it indicates that the

collision-induced subduction transference during Tethyan evolution should not be so easy, because the multiple Tethyan Oceans generally have an old and thick lithosphere at the passive margin (*Stampfli and Borel*, 2002; *Müller et al.*, 2008; *Stampfli*, 2013). In this study, we aim to combine the models with terrane collision/accretion and SI at the passive margins, in order to understand the dynamics of collision-induced subduction transference as well as the key point of Tethyan evolution.

Another important issue for the collision-induced subduction transference is the time span between the terrane collision and SI in the neighboring plate. In the Tethyan system, for example, the collision of the Qiangtang-Lhasa terrane, which occurred in Early Cretaceous (~140 Ma), may trigger the northward SI (~137 Ma) of the Indus-Yarlung Zangbo Tethyan ocean, i.e. a branch of the Neo-Tethys (*Zhu et al.*, 2013). The time for the collision between the Iranian terrane and Eurasia was at about 228~201 Ma, whereas the neighboring SI at about 187 Ma (*Wan et al.*, 2019), which indicates the SI occurring at about 20 Myrs after the collision. Notably, the times and time spans between collision and neighboring SI in Tethyan system are not well constrained due to the vague geological records. Specially, the Indian Oceanic plate does not begin subduction after the India-Eurasia collision for >50 Myrs, which makes it even more difficult to answer the question from geological observations (*Niu et al.*, 2003; *Stern*, 2004; *Stern and Gerya*, 2018).

The required conditions and time scales of collision-induced subduction transference are rarely studied and thus remain unresolved. In order to study these problems, systematical numerical models are conducted with variable properties of converging plates and different boundary conditions. The model results are further compared with the geological records of Tethys and shed new lights on the Tethyan dynamic evolution as well as the plate tectonic theory.

2 Initial Model Setup

2.1 Original model setup

The 2-D original model is 4000 km in length and 1400 km in depth, as shown in Figure 2a. The model includes two oceanic plates and two continental plates. A spreading oceanic plate (1000 km) is configured on the left side of the model, which is neighbored by a drifting continental terrane (1000 km). Another oceanic plate (600 km) is set between the drifting continental terrane and the overriding continental plate (1400 km). A weak zone is initially applied between the subducting oceanic plate and the overriding continental plate. Wet olivine rheology is applied for the weak zone, whereas dry olivine rheology is used for normal mantle rocks (*Karato and Wu*, 1993). The crust of continental plate is set to be 35 km, including a 20 km thick upper crust and a 15 km thick lower crust. For the drifting continental plate, the lithospheric thickness is set to be 100 km, whereas the overriding continental lithosphere is 140 km thick. The oceanic lithosphere is composed of a 3 km thick basalt layer as the upper crust, a 5 km thick gabbro layer as the lower crust, as well as a lithospheric mantle layer with the thickness dependent on the age (*Turcotte and Schubert*, 2002). The subducting oceanic plate is 100 km in thickness and 180 Ma in age, whereas the age of spreading oceanic plate is varied in the numerical studies. A ‘stick air’ layer is applied on the top of the model to allow the deformation of the crustal surface (*Schmeling et al.*, 2008; *Crameri et al.*, 2012). In the model, a ‘stick air’

layer of 10 km thick is set above the continental plate and 12 km above the oceanic plate, in order for the gravity isostasy.

The temperature conditions of the top and bottom boundaries are fixed, with 273 K and 2248 K, respectively. The left and right boundaries are adiabatic, with no heat flux across them. For the thermal structure of oceanic lithosphere, half-space cooling model is applied (e.g., *Turcotte and Schubert*, 2002). For the continental lithosphere, a linear temperature gradient is applied with 273 K on the surface and 1623 K at the bottom of lithosphere. An adiabatic temperature gradient of 0.5 K/km is applied for the sub-lithospheric mantle. The phase transitions at 410 km and 660 km are applied (*Li et al.*, 2019), with the Clapeyron slopes of 2.5 MPa/K and -1.0 MPa/K, respectively.

All the velocity boundary conditions of the model are set to be free slip. The subducting plate is pushed with a constant velocity (v_x = 10 cm/yr) in the left side of the spreading oceanic plate and the middle of drifting continental terrane, as shown in Figure 2a with two orange rectangles and arrows. The same constant convergent velocities are applied for 6 Myrs in the original model in order to avoid deformation in the passive margin between spreading oceanic plate and drifting continental plate.

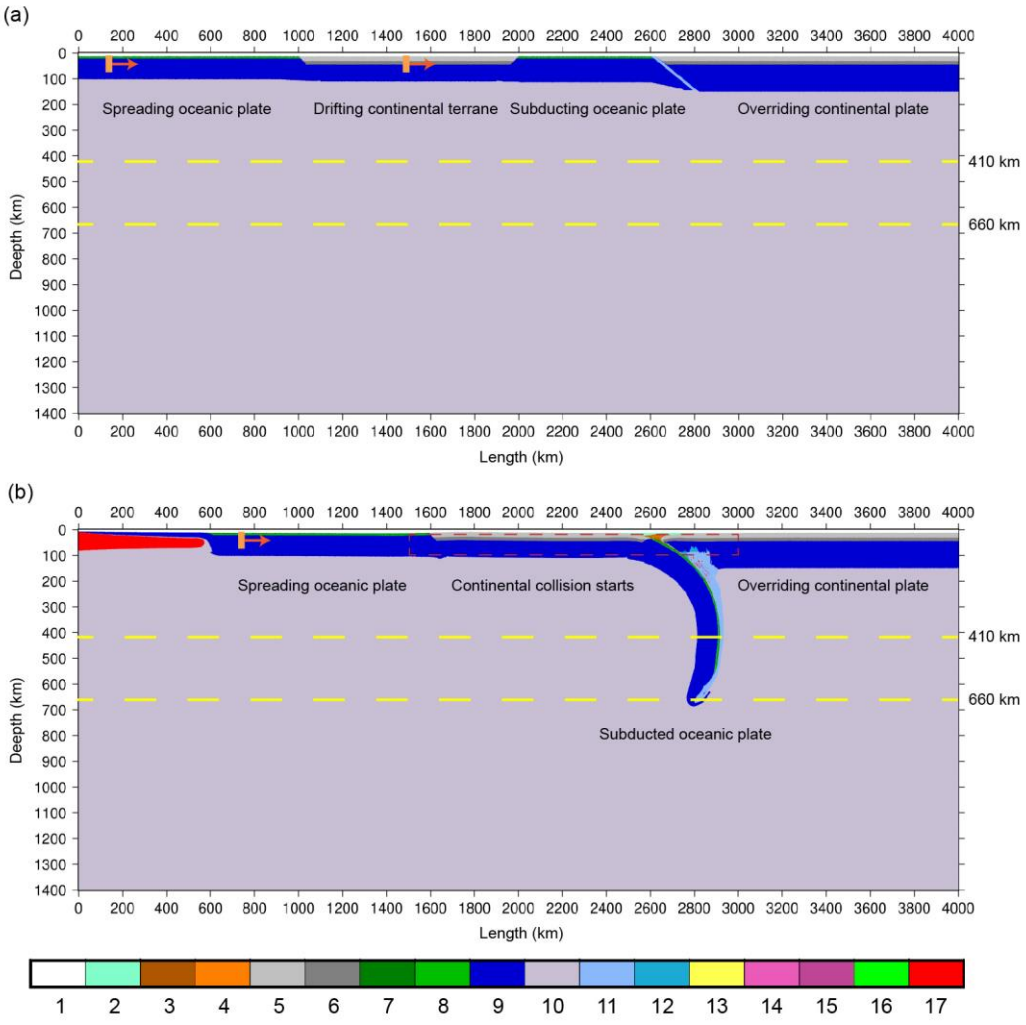

Figure 2. (a) Original model configuration with an overriding continental plate, a subducting oceanic plate and an initial weak zone in between. Wet olivine rheology is applied for the weak zone, whereas dry olivine rheology is used for normal mantle rocks (*Karato and Wu*, 1993). A drifting continental terrane is incorporated in the oceanic plate. The subducting plate is pushed at two different positions as marked by the orange rectangles and arrows, with the same and constant velocity (v_x = 10 cm/yr). **(b)** The beginning of continental collision after 6 Myrs with total convergence of 600 km. This snapshot is used as the initial model for the following study, which is either pure free subduction without any pushing, or pushed by a constant force at the left tip of the spreading oceanic plate. The yellow dashed lines denote the 410 km and 660 km discontinuities. Colors indicate the rock types, specified by the color grid: 1, stick air; 2, sea water; 3,4, sediments; 5,6, continental upper and lower crust, respectively; 7,8, oceanic upper and lower crust, respectively; 9, lithospheric mantle; 10, asthenosphere, 11, hydrated mantle; 12, serpentinized mantle; 13, partially molten sediments; 14, partially molten continental upper crust; 15, partially molten continental lower crust; 16, partially molten oceanic crust; 17, partially molten mantle.

2.2 Model setup and boundary conditions from collision

The original model in Figure 2a is pushed by a constant velocity of 10 cm/yr for 6 Myrs, with a total convergence of 600 km. It leads to a snapshot with the beginning of continental collision, as shown in Figure 2b, after which the previous boundary conditions with constant convergent velocity are cancelled. Thus, the original model driven by boundary velocity is only used for the first subduction and provides the slab pull force for the further evolution of the model.

In the following study, the initial collision snapshot (Figure 2b) is employed as the initial model. Two different types of boundary conditions are further applied and compared. One is the self-consistent free subduction driven purely by the slab pull, i.e. no pushing anywhere. Another one is pushed by a constant force at the left tip of the spreading oceanic plate (Figure 2b), the effect of which is combined with the slab pull from the subducted slab. The conditions for the SI of spreading oceanic plate after the continental collision will be systematically studied.

Detailed numerical methodologies (i.e. governing equations, rheological flow laws, phase transitions, hydration and partial melting) are shown in the supporting information and following *Li et al.* (2019).

3 Model Results

3.1 Free subduction after collision

In this set of models, no prescribed convergent boundary conditions are applied after the initial collision. In order to study the collision-induced subduction transference and SI at the passive margin, two different models with contrasting rheological strengths of passive margin are applied. In Model-1, no weak zone is prescribed (Figure 3a). In Model-2, an initial weak zone with wet olivine rheology (*Karato and Wu*, 1993) is applied in the ocean-continental transition (OCT) zone (Figure 3b).

The evolutions of these two models are similar before the slab break-off (c.f. Figures 3a and 3b). The dehydration occurs during the previous subduction of the oceanic crust, which results in a weak subduction channel. The drifting continental lithosphere subducts under the fixed overriding continental plate, driven by the slab pull from the subducted oceanic plate. However, due to the low density, a part of the continental crust is detached and exhumed to the surface or the crustal level. Another part of continental crust could be dragged into the mantle. The buoyancy of subducted continental crust competes with the slab pull from sinking oceanic pate. Finally, the slab break-off occurs around the OCT. Consequently, the subducted continental plate migrates upward with the loss of slab pull (i.e. eduction) (*Duretz et al.*, 2012), which pushes the neighboring passive continental margin and modifies the stress and strain rate fields as shown in Figures 4a and 4b. In Model-1 without any prescribed weak zone, the eduction-induced deformation is rather limited that no clear sign for SI can be observed (Figure 3a). There is no significant deformation or stress localization in the neighboring passive margin after the break-off (Figure 4a). In Model-2 with a prescribed weak zone, an incipient subduction initiates at the beginning (Figure 3b), which stops a short time later due to the limited pushing from eduction. The deformation and stress localization emerge in the neighboring passive margin corresponding to the inception of SI, which however quickly fades with time (Figure 4b). Thus, the collision-induced subduction transference is not applicable in such cases with free subduction after collision (Figure 3).

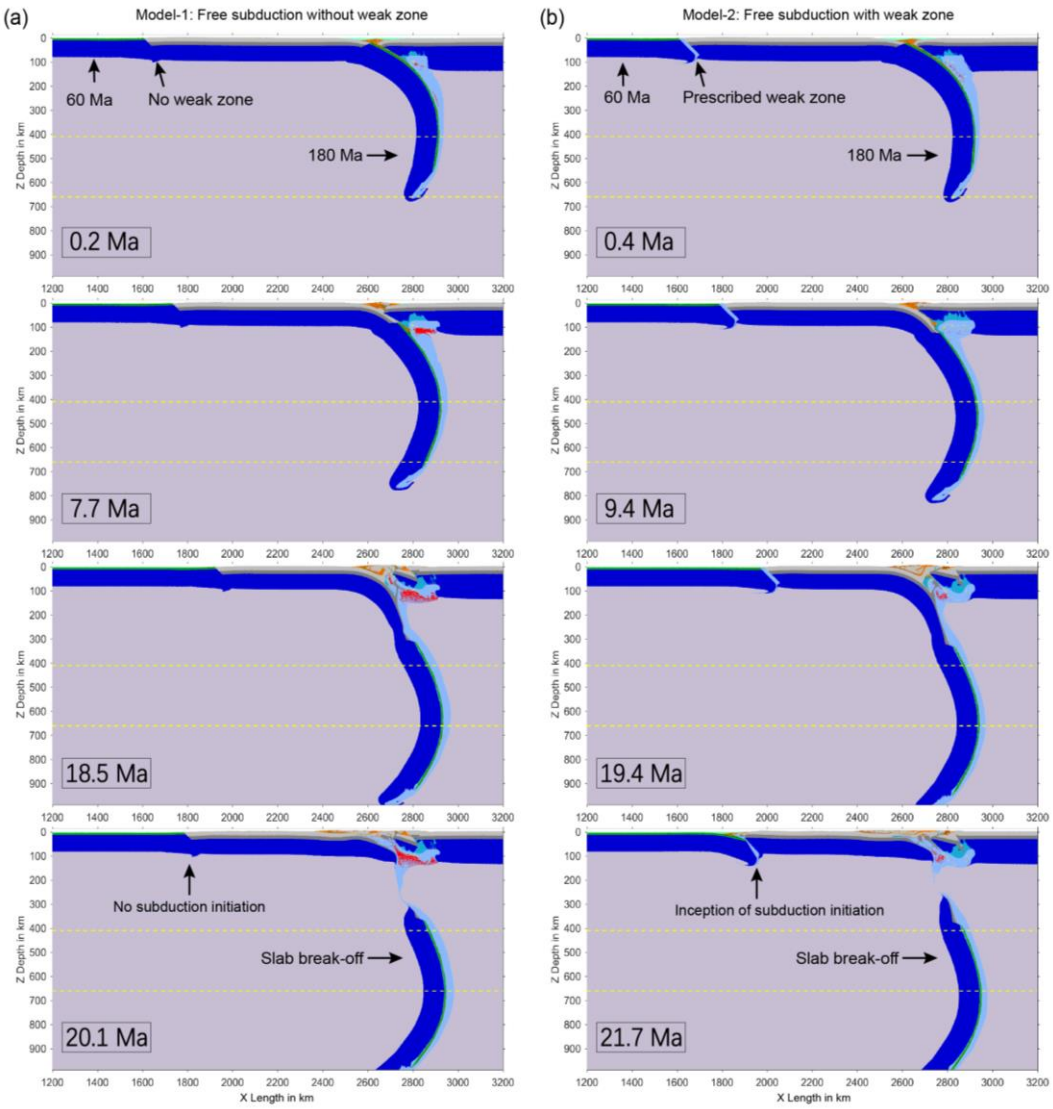

Figure 3. Models of free subduction after collision, with colors indicating rock types as shown in Figure 2. **(a)** Evolution of Model-1 without prescribed weak zone at the passive margin. **(b)** Evolution of Model-2 with a prescribed weak zone at the passive margin.

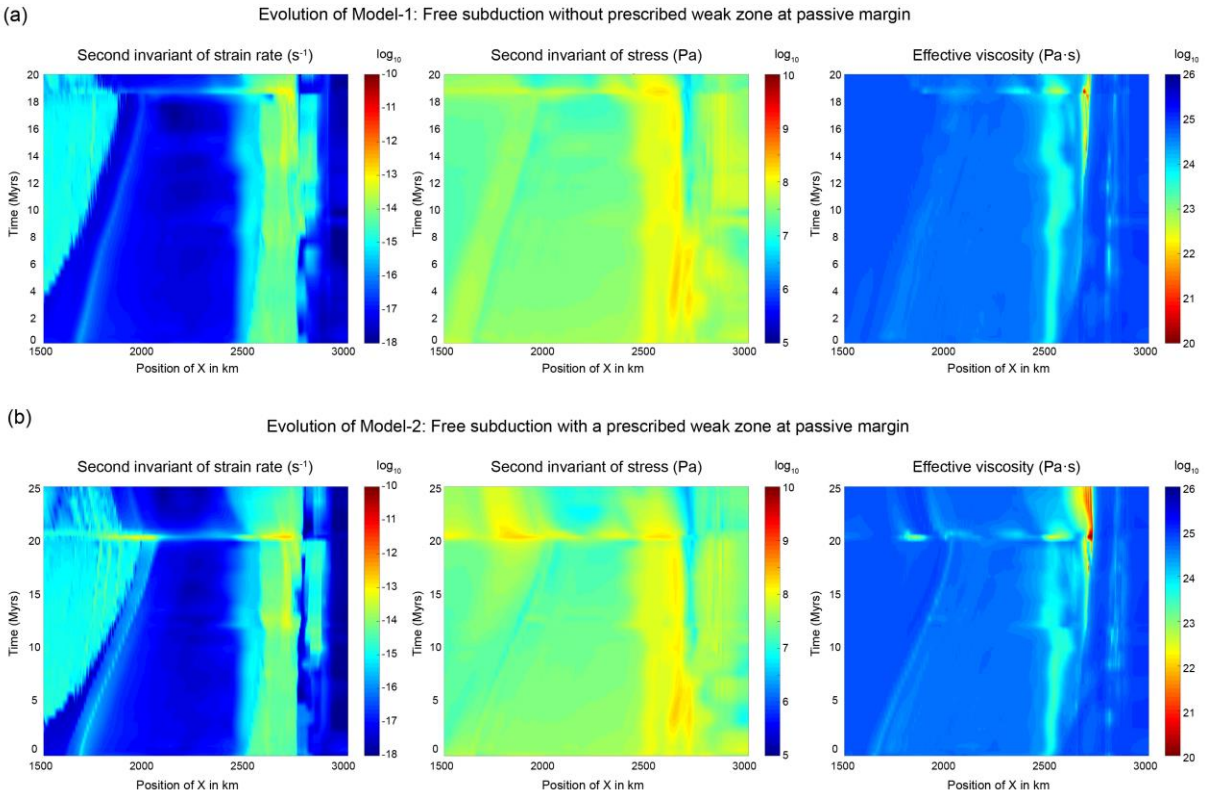

Figure 4. The time-dependent evolution of strain rate, stress and viscosity fields. The position of the profile (X = 1500~3000 km) is indicated by the red box in Figure 2b, with values of second invariant of strain rate and stress, as well as the effective viscosity averaged with depth. **(a)** Evolution of Model-1 without prescribed weak zone at the passive margin, same as Figure 3a. **(b)** Evolution of Model-2 with a prescribed weak zone at the passive margin, same as Figure 3b.

3.2 Forced subduction after collision

In nature, a horizontal plate without connecting to any subducting slab could also be dragged to move by the pushing from mid-ocean ridge and shearing from the mantle convection (*Turcotte and Schubert*, 1982; *Niu et al.*, 2003; *Mahatsente*, 2017; *Sun*, 2019). In this section, we conduct systematic numerical models with a constant convergent force employed on the spreading oceanic plate (Figure 2b) to investigate the conditions and time scale of collision-induced subduction transference. The models are classified into two groups, i.e. without or with a prescribed weak zone at the passive margin.

3.2.1 No prescribed weak zone at the neighboring passive margin

Systematic numerical models are conducted with variable convergent boundary forces and variable ages of the spreading oceanic plate (Figure 5). The model results indicate that the collision-induced SI at the neighboring passive margin requires a relatively high boundary force, i.e. $>8.0\times10^{12}$ N/m, which slightly increases with older oceanic lithosphere. If the boundary force is larger enough for a specific passive margin, the SI generally occurs within 10 Myrs after the

initial collision (Figure 5). This time scale of SI is also dependent on the boundary force, i.e. the larger boundary force resulting in earlier SI occurrence.

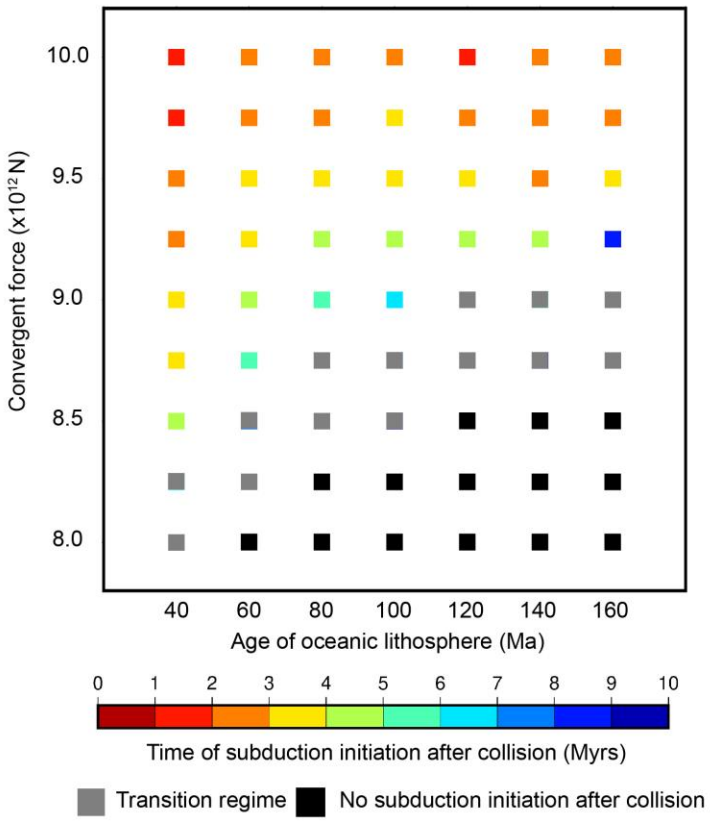

Figure 5. The occurrence and time scale of subduction initiation after collision, dependent on the convergent boundary force and the age of oceanic lithosphere.

The detailed evolutions of two representative models are further demonstrated, i.e. Model-3 with oceanic lithosphere of 80 Ma and boundary force of 9.0×10^{12} N/m, as well as Model-4 with oceanic lithosphere of 80 Ma and boundary force of 8.5×10^{12} N/m (Figures 6 and 7). In Model-3, the SI occurs at the neighboring passive margin during subduction of the continental terrane, at about 4 Myrs after initial collision. The evolution of stress field (Figure 7a) demonstrates a significant stress localization at X=1600-2000 km, i.e. around the OCT in the neighboring passive margin (Figure 6a). This process lasts for about 2 Myrs and finally leads to SI with high strain rate and release of stress (Figure 7a).

As a comparison, the relatively low boundary force in Model-4 prevents the collision-induced SI at the neighboring passive margin (Figure 6b). In this regime, the general stress building occurs slowly and in a wider region, which leads to weak strain localization in the neighboring passive margin (Figure 7b). Thus, the SI is not predicted. In more details, there are two peak stress localization processes around the passive margin. The first one occurs at about 10 Myrs after collision, which is corresponding to the detachment and exhumation of the subducted continental crust. However, it just lasts for a short time and does not result in SI. The

later stress localization occurs at around 30 Myrs (Figure 7b), corresponding to the slab break-off, which again does not lead to abrupt failure of the passive margin. Finally, although the extensive continental collision occurs for >30 Myrs, no SI is predicted at the neighboring passive margin.

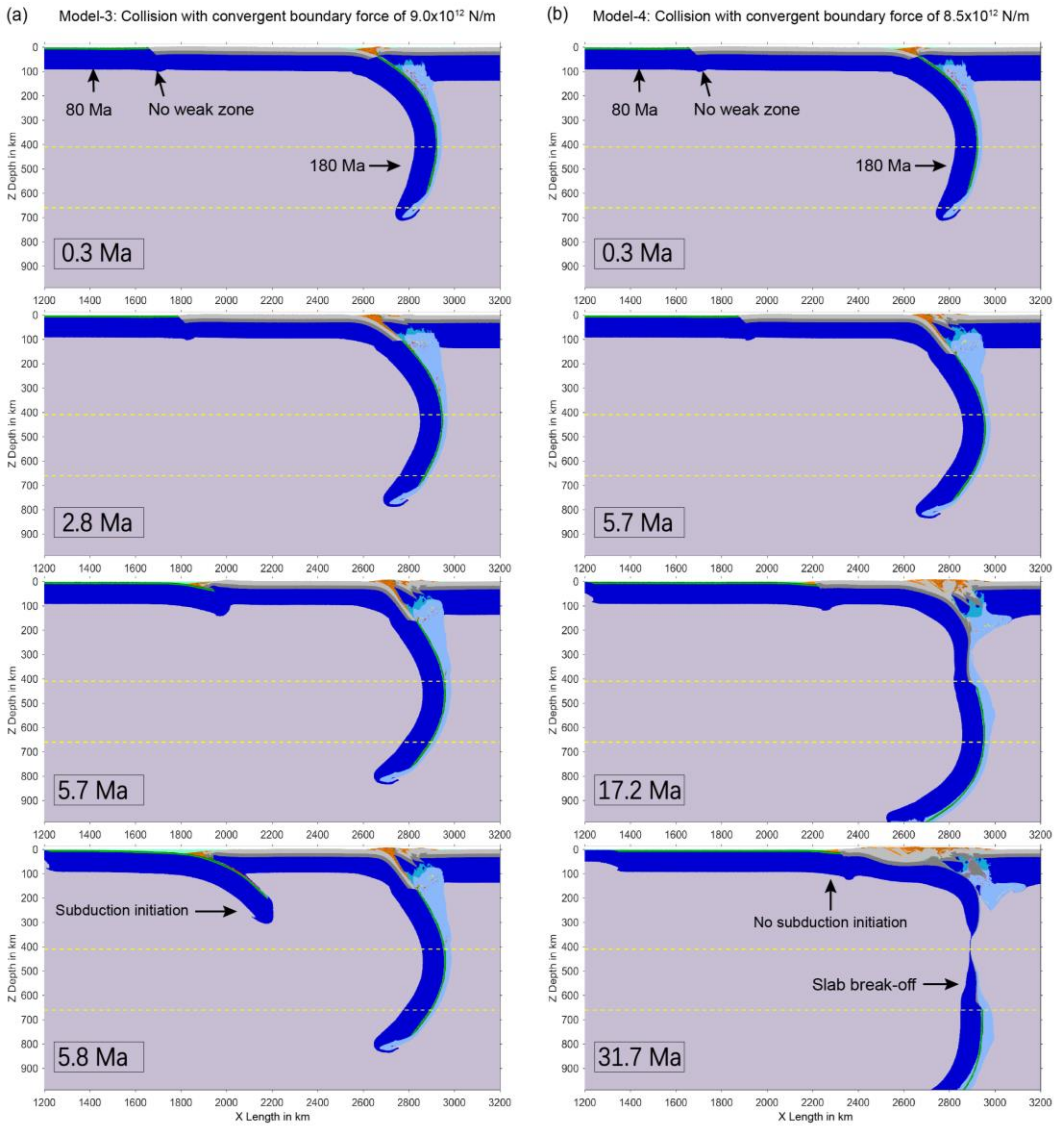

Figure 6. Models of forced subduction after collision, with colors indicating rock types as in Figure 2. No initial weak zone is prescribed at the passive margin. **(a)** Evolution of Model-3 with convergent boundary force of 9.0×10^{12} N/m. **(b)** Evolution of Model-4 with convergent boundary force of 8.5×10^{12} N/m.

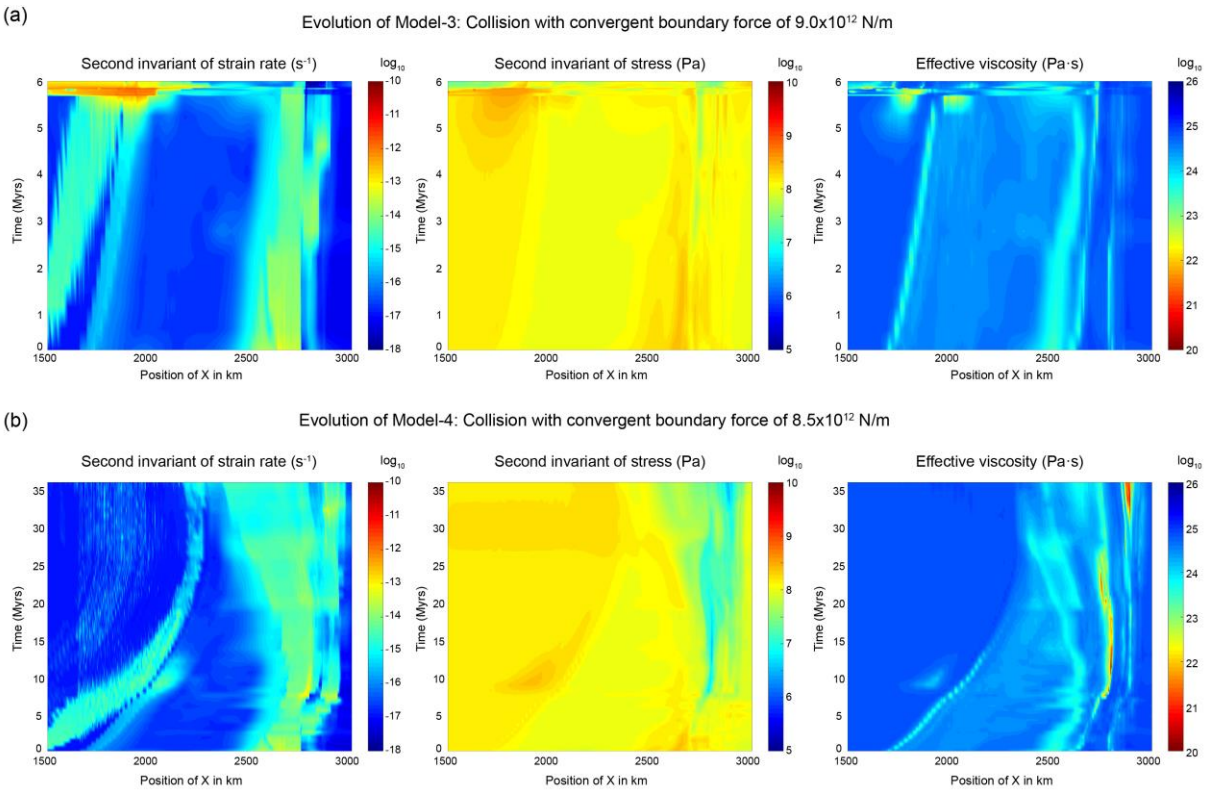

Figure 7. The time-dependent evolution of strain rate, stress and viscosity fields. The position of the profile (X = 1500~3000 km) is indicated by the red box of Figure 2b, with the values of second invariant of strain rate and stress, as well as the effective viscosity averaged with depth. **(a)** Evolution of Model-3 with convergent boundary force of 9.0×10^{12} N/m, same as Figure 6a. **(b)** Evolution of Model-4 with convergent boundary force of 8.5×10^{12} N/m, same as Figure 6b.

3.2.2 Existence of a prescribed weak zone at the neighboring passive margin

The existence of a prescribed weak zone at the passive margin dramatically reduces the required convergent force for SI after collision. For example, the boundary force required for SI at the neighboring passive margin with 60 Ma oceanic lithosphere is ~4.0×10^{12} N/m (Figure 8), which is about half of that in the models without weak zone. Two modes of SI are obtained according to systematic numerical studies, which are the earlier SI after initial collision and the later SI after slab break-off (Figure 8). In the models with younger oceanic plate and relatively larger boundary force, the SI results immediately after the initial collision. In contrast with older oceanic plate and relatively smaller boundary force, the SI occurs much later after the slab break-off. It is worth noting that the models with very low convergent forces encounter serious problems in the solver convergence, which thus prevents obtaining models without SI in this regime.

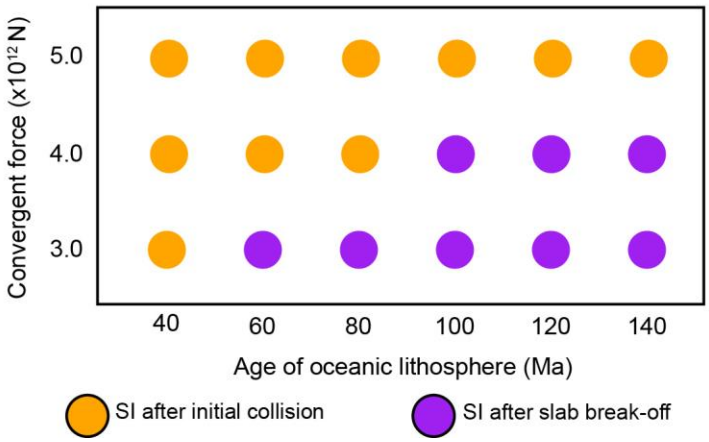

Figure 8. Two contrasting modes of forced subduction initiation (SI) at the neighboring passive margin with a prescribed weak zone, i.e. earlier SI after initial collision versus later SI after slab break-off, dependent on the age of oceanic lithosphere and the convergent boundary force.

The evolution of two contrasting models are demonstrated in Figures 9 and 10, which are either SI after collision (Model-5 with oceanic lithosphere of 80 Ma and boundary force of 4.0×10^{12} N/m) or SI after slab break-off (Model-6 with oceanic lithosphere of 80 Ma and boundary force of 3.0×10^{12} N/m).

In Model-5, the SI occurs at the neighboring passive margin soon after the continental collision (Figure 9a). The significant stress localization in the passive margin leads to the failure of prescribed weak zone and the occurrence of SI (Figure 10a). The forced convergence is accommodated by both subduction zones, i.e. the old one on the right and the newly formed one on the left (Figure 9a). However, through the model evolution, the strain rate in the old subduction zone decreases, whereas that in the new subduction zone increases (Figure 10a). It indicates the dominance of convergence switches gradually from the old subduction zone to the new one.

In Model-6, the relatively low convergent force is not enough to trigger SI immediately after collision (Figure 9b). Although SI does not occur, there is still deformation localized in the weak zone after collision, which is clearly demonstrated by the stress building and resulting higher strain rates (Figure 10b). However, the deformation in the passive margin is too slow for the occurrence of SI. At about 18.5 Myrs after collision, the slab break-off occurs with eduction of continental plate, which results in an additional push on the neighboring passive margin. Finally, the SI is induced, which is further sustained by the continuous convergent boundary force.

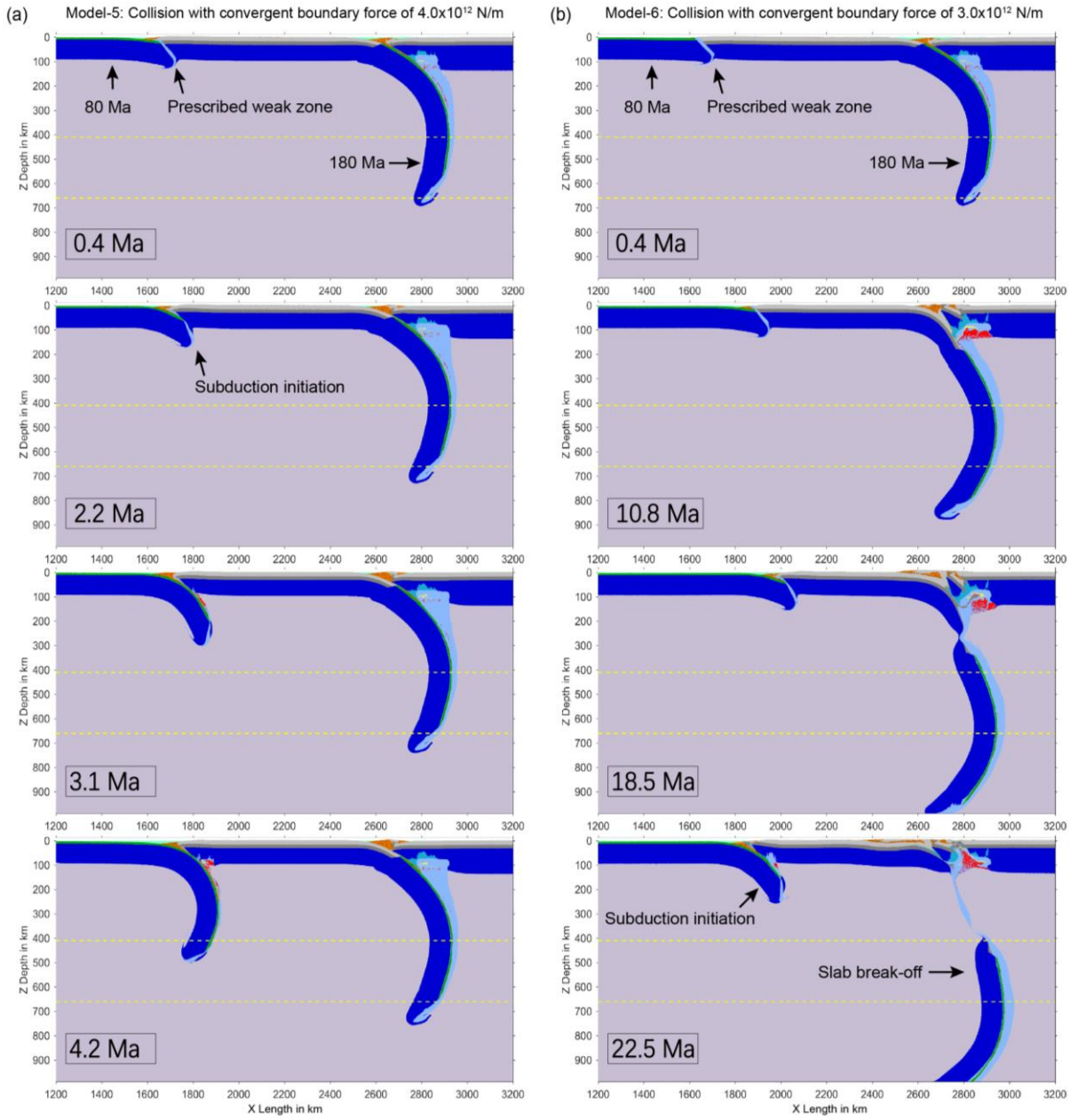

Figure 9. Models of forced subduction initiation at the neighboring passive margin with a prescribed weak zone, with colors indicating rock types as in Figure 2. **(a)** Evolution of Model-5 with convergent boundary force of 4.0×10^{12} N/m. **(b)** Evolution of Model-6 with convergent boundary force of 3.0×10^{12} N/m.

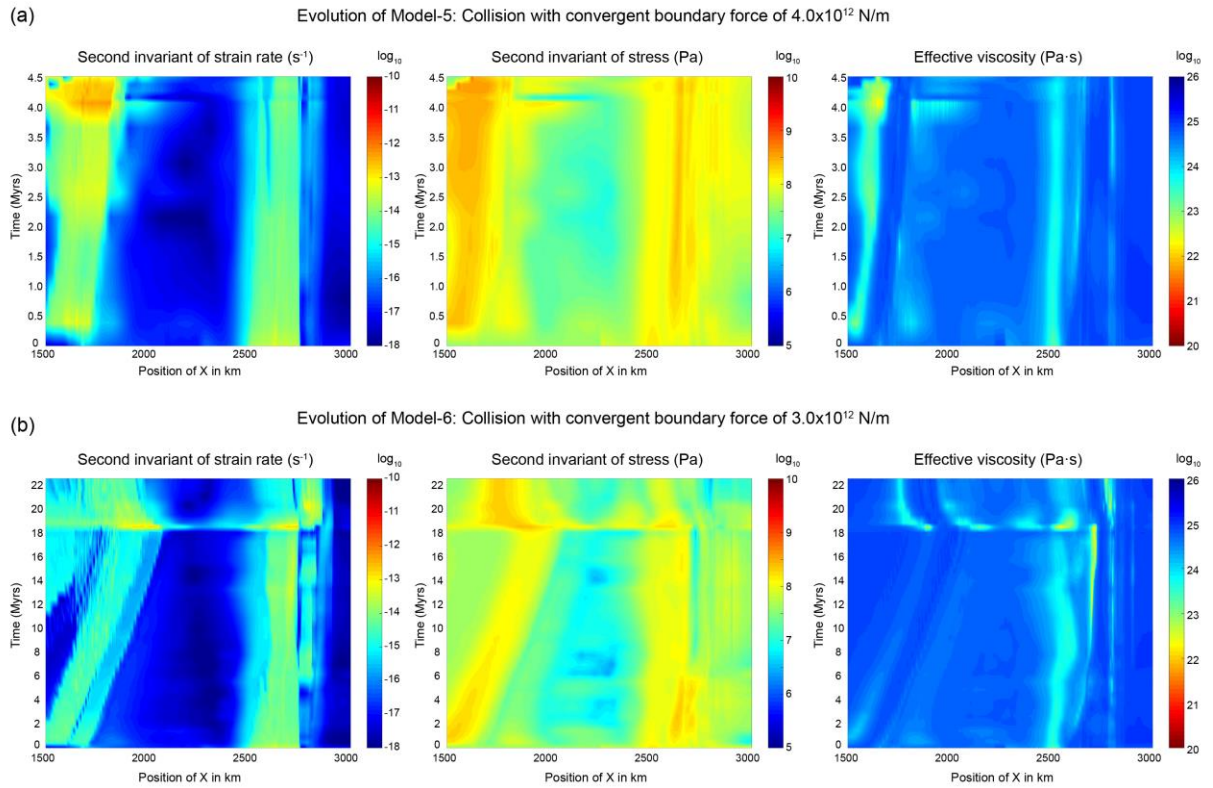

Figure 10. The time-dependent evolution of strain rate, stress and viscosity fields. The position of the profile (X = 1500~3000 km) is indicated by the red box of Figure 2b, with values of second invariant of strain rate and stress, as well as the effective viscosity averaged with depth. **(a)** Evolution of Model-5 with convergent boundary force of 4.0×10^{12} N/m, same as Figure 9a. **(b)** Evolution of Model-6 with convergent boundary force of 3.0×10^{12} N/m, same as Figure 9b.

3.3 Effect of the length of accreted continental terrane

In the previous models, the length of drifting continental terrane within the subducting oceanic plate is constant of 1000 km. During the Tethyan evolution, the multiple terranes accreted to the Eurasian plate may be wider (e.g., Indian plate) or narrower (e.g., Lhasa terrane). However, it is worth noting that the Lhasa terrane is included in the Cimmerian block, the length of which is hard to constrain. In order to understand the effect of the terrane's length on the SI at the neighboring passive margin, comparable experiments are further conducted with shorter terrane of 500 km.

Model-7 and Model-8 are comparable to Model-3 (Figure 6a) and Model-4 (Figure 6b), respectively. The only difference is the application of a shorter drifting continental terrane (500 km). The evolutions of these two additional models are similar to Model-3 (Figure 6a), in which the SI occurs at the neighboring passive margin after the continental deep subduction (Figure 11). The comparisons between Model-8 (SI in Figure 11b) and Model-4 (no SI in Figure 6b) indicate that the shorter drifting continental terrane favors the collision-induced subduction transference.

In order to better understand the effects of continental terrane's length, we further conduct a set of numerical models with shorter continental terrane and compare them to the previous models with longer continental terrane (Figure 12). The results indicate that the length of drifting continental terrane does not play significant roles in the models with higher boundary forces. However, in the regime with lower boundary forces, the collision of a shorter continental terrane leads to SI a bit earlier (by 0~2 Myrs) and easier (by decreasing the required boundary force of 0.6×10^{12} N/m) than a longer one (Figure 12).

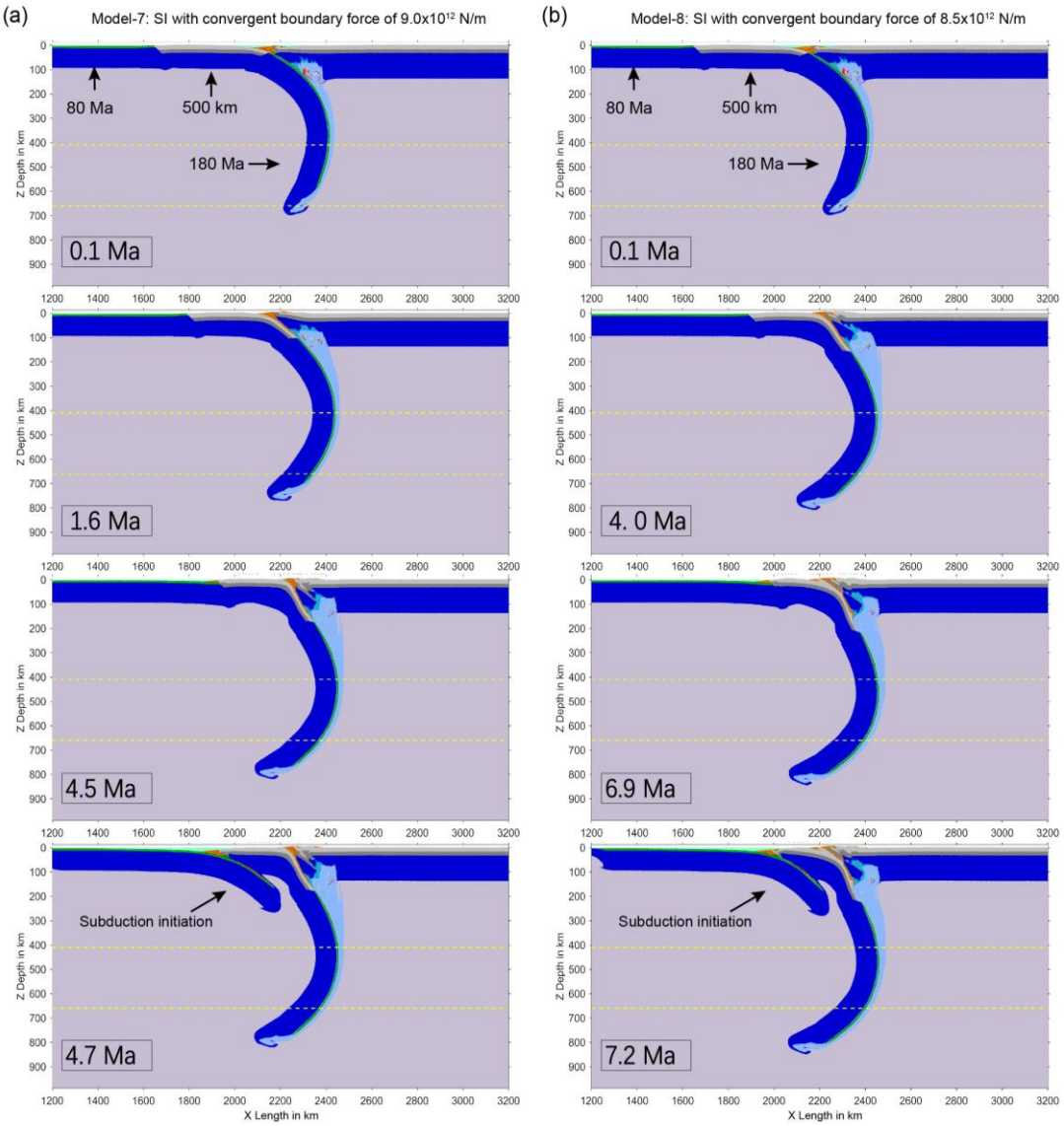

Figure 11. Models with shorter drifting continental terrane of 500 km, with colors indicating rock types as in Figure 2. **(a)** Evolution of Model-7 with convergent boundary force of 9.0×10^{12} N/m, comparable to Model-3 in Figure 6a. **(b)** Evolution of Model-8 with convergent boundary force of 8.5×10^{12} N/m, comparable to Model-4 in Figure 6b.

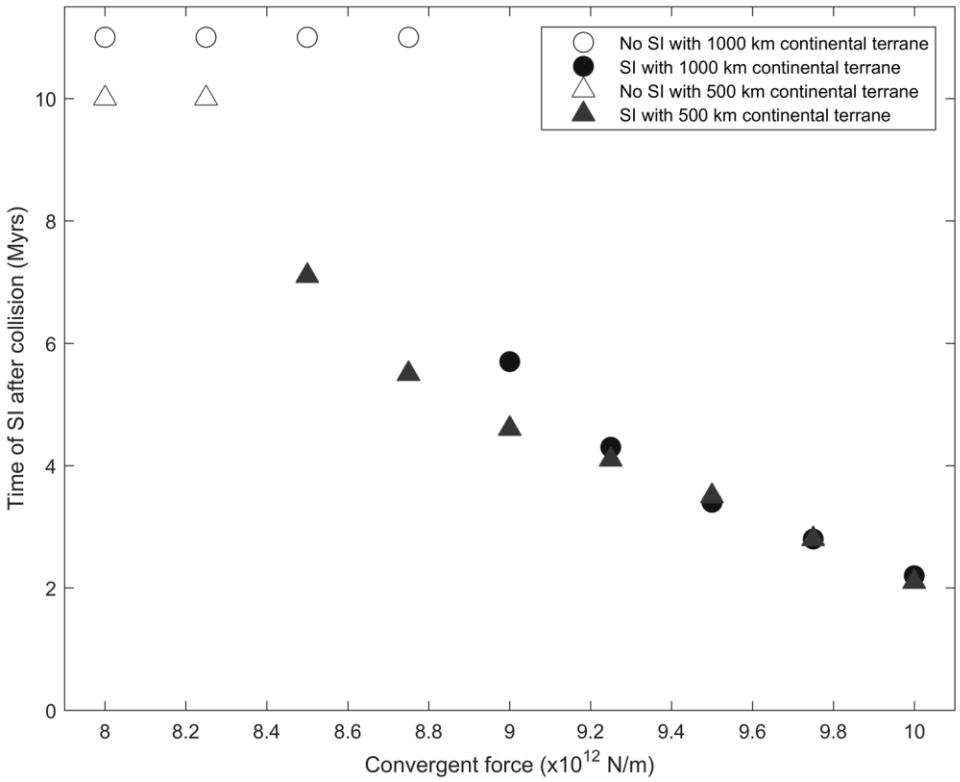

Figure 12. Comparisons among models with shorter (500 km) and longer (1000 km) drifting continental terranes. The circles show the results of numerical models as in Figure 5 with spreading oceanic plate of 80 Ma and longer continental terrane of 1000 km, whereas the triangles for the comparable models with shorter continental terrane of 500 km. All the other parameters are identical.

3.4 Effect of the length of the firstly subducted oceanic slab

In the previous models, the length of the firstly subducted oceanic slab is constant of 600 km, which leads to the slab arriving at around 660 km discontinuity, i.e. the boundary between the upper and lower mantles. Further varying the length of subducted slab may play a role in modifying the force of slab pull. In order to test its effects on the SI at the neighboring passive margin, additional experiments are conducted with longer subducted oceanic slab of 1000 km (Figures 13, 14).

In the regime with relatively lower convergent force of 8.5×10^{12} N/m, the evolution of Model-10 is very similar to Model-4 although with difference lengths of subducted slab (c.f. Figures 13b and Figure 6b). No SI is predicted at the neighboring passive margin of both models. Alternatively, in the regime with relatively higher convergent force of 9.0×10^{12} N/m, the collision-induced SI at the passive margin occurs a bit later for ~2 Myrs in Model-9 with a longer subducted oceanic slab of 1000 km than that in Model-3 with a shorter subducted slab of 600 km (c.f. Figures 13a and Figure 6a). Figure 14 further summarizes and illustrates the effects of subducted slab length on the time of SI at the neighboring passive margin. It indicates that the time of SI after collision is generally later (by ~2 Myrs) in the models with a longer subducted

slab of 1000 km than those of 600 km, because the larger slab pull delays the stress building and lithospheric collapse. However, the length of subducted slab does not affect the threshold of convergent force required to trigger SI at the neighboring passive margin. Thus, it plays secondary roles in the collision-induced subduction transference.

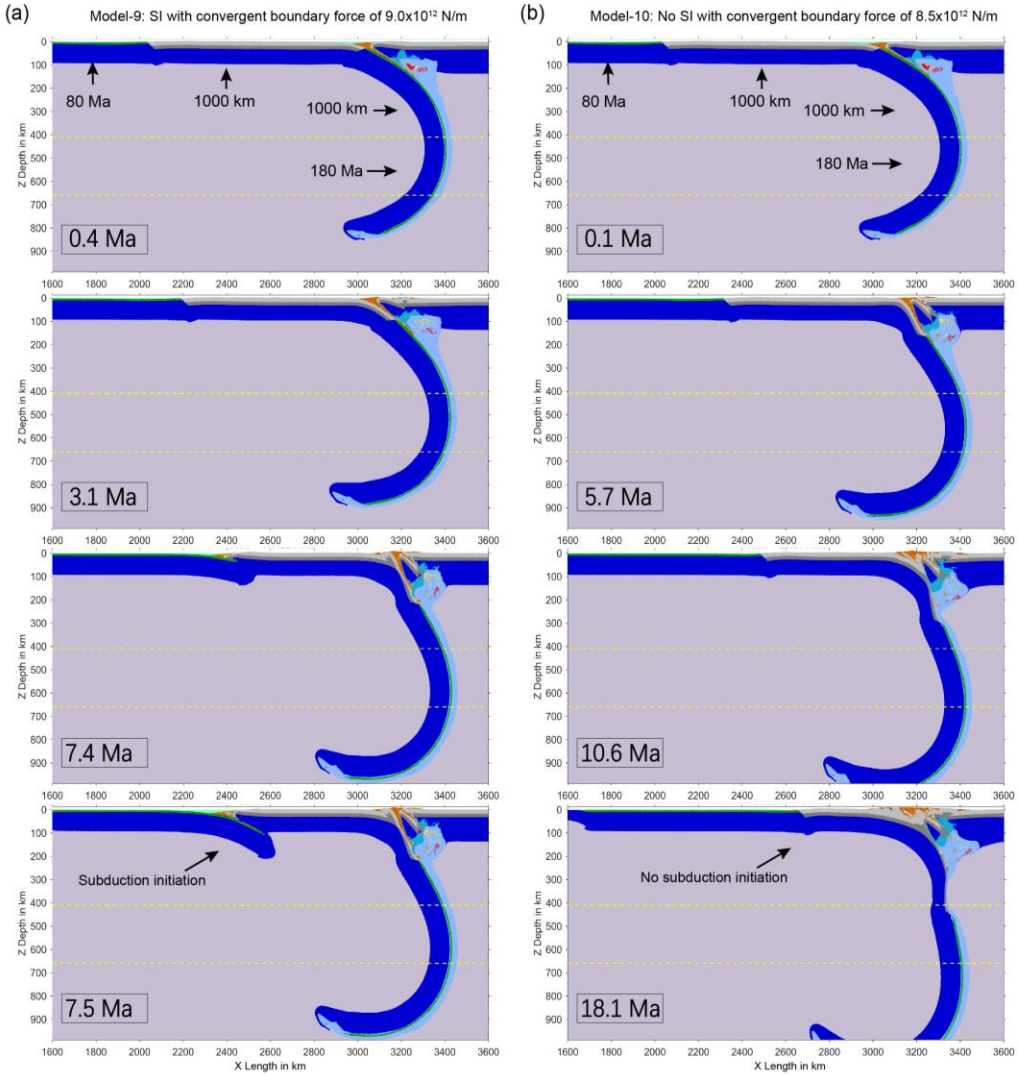

Figure 13. Numerical models with subducted oceanic plate of 1000 km. All the other parameters are comparable to Model-3 and Model-4, respectively (Figure 6). The colors indicate rock types as in Figure 2. **(a)** Evolution of Model-9 with convergent boundary force of 9.0×10^{12} N/m. **(b)** Evolution of Model-10 with convergent boundary force of 8.5×10^{12} N/m.

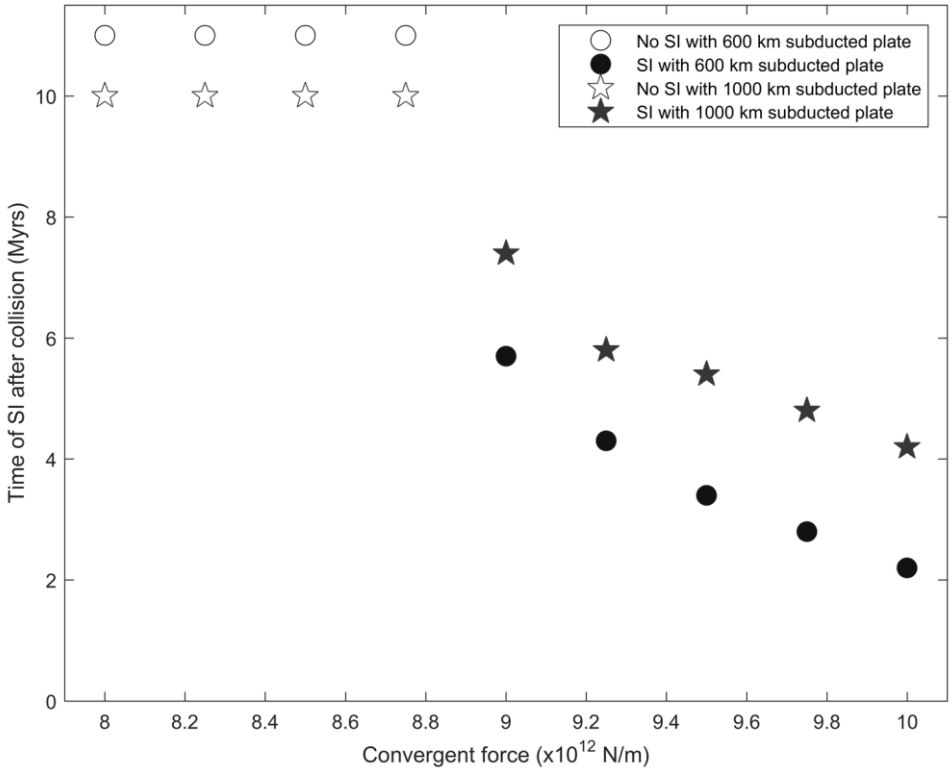

Figure 14. Comparisons among models with shorter (600 km) or longer (1000 km) subducted oceanic plate. The circles show the results of numerical models as in Figure 5 with spreading oceanic plate of 80 Ma and subducted oceanic plate of 600 km, whereas the stars for the comparable models with longer subducted oceanic plate of 1000 km. All the other parameters are identical.

4 Discussion

4.1 Controlling factors of collision-induced subduction transference

The collision-induced subduction transference is a complex dynamic process, which is affected by not only the present subduction/collision itself, but also the properties of the neighboring passive margin and the boundary conditions. The current numerical models indicate that the resistance of convergence from continental collision leads to stress building in the neighboring plate and passive margin (e.g., Figures 4 and 7). On the other hand, the slab break-off and the resulting eduction can trigger the incipient SI at the neighboring passive margin (e.g., Figures 3b and 9b). However, the steady SI and the final development of mature subduction require additional forces, e.g., the boundary convergence force. In Model-2 without boundary force (Figure 3b), the incipient SI does not evolve into a self-sustained subduction zone because of the short and limited convergence from slab break-off. In contrast, the similarly induced SI is sustained by the convergent force in Model-6 (Figure 9b). Thus, the convergent force on the drifting oceanic plate is a critical factor for the occurrence of collision-induced subduction transference. In addition, the increasing of convergent force could extensively reduce the time for SI after collision, as shown in Figure 5.

The rheological strength of the passive margin is controlled by the age of neighboring oceanic lithosphere as well as the possible presence of weak zones. The numerical models indicate that the collision-induced SI at the passive margin without weak zone generally requires a high convergent force of above 8.0×10^{12} N/m (Figure 5). However, the force of ridge push is estimated to be around 3.0×10^{12} N/m (*Harper*, 1975; *Turcotte and Schubert*, 1982; *Ghosh et al.*, 2006; *Mahatsente*, 2017; *Sun*, 2019), which is not large enough for the collision-induced SI. The existence of a weak zone with wet olivine rheology (*Karato and Wu*, 1993) at the OCT can significantly reduce the required convergent force for SI after collision (Figure 8), i.e. no higher than $3.0\sim5.0\times10^{12}$ N/m. On the other hand, the age of the neighboring oceanic plate plays a second-order role in the collision-induced subduction transference, comparing to effects of weak zone and boundary force, although the required force for triggering SI increases slightly with the oceanic lithospheric age in both models with and without weak zones (Figures 5 and 8). The effects of oceanic age are two-folded, i.e. on viscosity and density, respectively. In the viscosity aspect, the old oceanic lithosphere increases the thickness and rheological strength of the passive margin, which leads to difficulty in its collapse and further SI. In the density aspect, the negatively buoyancy of oceanic plate increases with age and thus contributes to the gravity instability and further the SI. However, the increase of strength and resistance to SI dominates, which finally results in the positive correlation between the oceanic age and the required convergent force for SI at the neighboring passive margin (Figures 5 and 8).

4.2 Implications for the dynamics of Tethyan evolution

The Tethyan system is a large scale and long living orogenic system on the Earth since the Paleozoic. The most special and intriguing character of Tethys is the multiple terranes or microcontinents drifting from Gondwana, and accreting to the Eurasia (or Laurasia) continent (Figure 1c) (*Wan et al.*, 2019). The drifting and collision processes of the Galatian supercontinent and the following SI of the Paleo-Tethys in the Early Paleozoic are much far away from present and consequently not well constrained from the geological records. Thus, we focus on the collision of the Cimmerian terranes with Eurasia and the following SI of the Neo-Tethys. More geological records can be obtained to constrain this collision-induced subduction transference.

The Neo-Tethyan tectonic belt is very long for ~10,000 km from the Western Europe to the Southeastern Asia. Here we focus on the regions with relatively well constrained geochronologic data, as shown in Figure 15. In the middle Tethys, the collision of Iranian block with the Eurasia is recorded by the deformation of early Mesozoic strata in Fariman basin, which indicates the time of collision is around 228-201 Ma (*Wan et al.*, 2019; *Zanchi et al.*, 2016). The subduction of the neighboring Neo-Tethyan oceanic plate in Iranian region started at about 200 Ma (*Wilmsen et al*., 2009), which was a bit later than the collision. Alternatively, for Tibetan Plateau, the collision between Cimmeria and Eurasia occurred at about 220-210 Ma, while the SI in this region was at about 205 Ma (*Wan et al.*, 2019; and references therein). Further to the east, the collision between the Sibumasu and Indo-China (part of Eurasia at that time) occurred at about 240 Ma, while the SI at the neighboring Neo-Tethyan Ocean was about 230 Ma (*Metcalfe*, 2013). As a summary, the SI of Neo-Tethys is generally following the collision of Cimmerian plates with Eurasia, with a time delay of <20 Myrs as shown in Figure 15. It is worth noting that various geological records are previously used as the proxy for the start of collision, e.g., the

exhumation of eclogite, the strata deformation, the metamorphic rocks, etc. Thus, the timing of collision is a bit varied among different studies (*Yin and Harrison*, 2000; *Aitchison et al.*, 2007; *Najman, et al.*, 2010; *DeCelles et al.*, 2014; *Zhu et al.*, 2015; *Searle*, 2019). On the other hand, the geological records for SI are even more complex (*Stern*, 2004; *Stern et al*., 2012; *Hall*, 2018; *Guilmette et al*., 2019; *Searle*, 2019; *Patriat et al.*, 2019; *Parlak et al.*, 2019). The emplacement of magmatic rock is generally later, by several million years, than the exact time of SI (*Hall*, 2018; *Shervais et al.*, 2019; *Arculus et al.*, 2019). Thus, the timing of SI may be delayed according to the magmatic records. The current numerical models indicate that the SI occurs in the neighboring plate within 10 Myrs after collision, under the favorable conditions of collision-induced subduction transference (Figure 5). Considering all the uncertainties as discussed above, the numerical models are consistent with the observations in the middle-eastern Tethys (Figure 15).

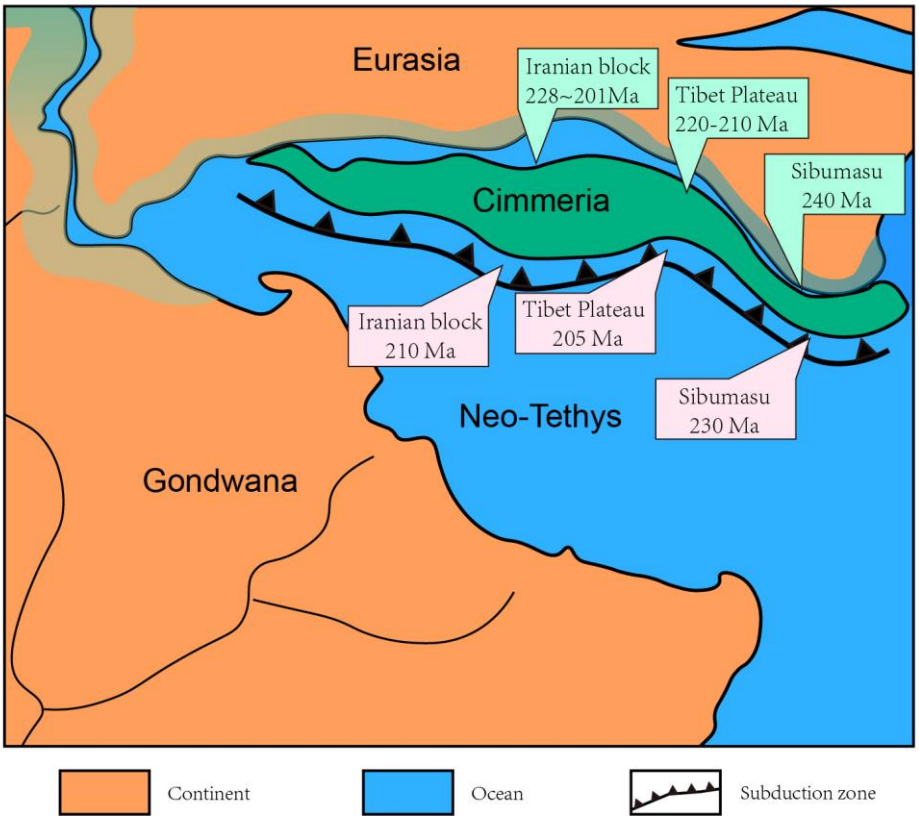

Figure 15. The conceptual model of subduction transference during the collision between Cimmerian terranes and Eurasian continent (modified after *Stampfli and Borel*, 2002). The numbers in the blue boxes show the estimated time of collision (*Metcalfe*, 2013; *Zanchi et al.*, 2016; *Wan et al.*, 2019), whereas those in the pink boxes indicate the time of subduction initiation of the Neo-Tethyan oceanic plate (*Wilmsen et al*., 2009; *Metcalfe*, 2013; *Wan et al.*, 2019).

Another issue for discussion is whether and when will the SI occur in the Indian Ocean as a response to the India-Asia collision, which is a challenging problem. The collision has already occurred for more than about 50 Ma (*Yin and Harrison*, 2000; *Aitchison et al.*, 2007; *Najman et*

al., 2010; *Lippert, et al.*, 2014; *Zhu et al.*, 2015; *Searle*, 2019); however, there is still no clear sign for the SI to the south of Indian continent, although some guesses have been suggested (*Niu et al.*, 2003; *Stern*, 2004; *Stern and Gerya*, 2018; *Pandey et al.*, 2019). Several reasons have been proposed for the absence of SI in the Indian ocean, although none has been confirmed, for example, the continuous shortening of overriding Tibetan plateau, the large width or the triangular shape of the Indian plate, the strength of an old and stable OCT (*Cloetingh*, 1989; *Stern*, 2004; *Stern and Gerya*, 2018). Based on our numerical models, the difficulty for the SI in the Indian Ocean may be due to the low convergent force and/or the lack of proper weak zones at the passive margin. The convergent force between the Indian plate and the Eurasian continent is estimated by the GPE to be about 3.0×10^{12} N/m (*Ghosh et al.*, 2006; *Schmalholz et al.*, 2014), which is lower than the required force for triggering SI for the neighboring Indian Oceanic plate with over 100 Ma lithosphere, if no weak zone is present (Figure 5). In this case, the convergence between plates is mainly accommodated by the deformation in the Himalayan collision zone, which is consistent with Model-4 (Figure 6b). On the other hand, the absence of SI in the Indian Ocean may also be a result of lack of proper weak zone according to our numerical models. The existence of weak zone is a common case on the Earth, which could be the faults, hydration zones and highly deformed/fracture zones (*Gurnis and Hall*, 2004; *Leng and Gurnis*, 2011; *Zhou et al.*, 2018; *Arcay et al.*, 2019). These weak zones may not collapse into subduction zone under the typical tectonic force of ridge push of about 3.0×10^{12} N/m (*Turcotte and Schubert*, 1982; *Mahatsente*, 2017) as shown in Figure 8. However, a short but strong impulse (e.g., slab break-off) can result in an incipient subduction zone, which is then sustained by a low convergent force (e.g., 3.0×10^{12} N/m) in Model-6 (Figure 9b). Obviously, the Indian plate has experienced the collision and slab break-off (*Yin and Harrison*, 2000; *Kohn and Parkinson*, 2002; *Aitchison et al.*, 2007; *Najman et al.*, 2010; *Zhu et al.*, 2015). The absence of SI may indicate the lack of proper weak zones in the Indian Oceanic plate to localize the incipient subduction.

5. Conclusions

The collision-induced subduction transference includes two aspects, i.e. the terrane collision/accretion and the subduction initiation (SI) at the neighboring passive margin, the dynamics of which are generally investigated individually. In this study, we combine these two regimes into an integrated model, and conduct systematic numerical experiments. The main conclusions include the following:

(1) The boundary force-driven convergence is required to trigger and sustain the SI at the neighboring passive margin after terrane collision and accretion. In contrast, the self-consistent force variations in the existing subduction/collision system (e.g., induced by continental subduction and/or slab break-off) are not enough for the subduction transference, although they can indeed trigger the incipient SI.

(2) The existence of weak zone at the passive margin can significantly promote the occurrence of SI, by decreasing the required boundary force to the reasonable value of plate tectonics. In addition, the age of oceanic lithosphere also plays a certain role by affecting the strength of passive margin, e.g., easier SI for younger oceanic plate under the same boundary force.

(3) The length of subducted oceanic slab or the accreting continental terrane plays secondary roles in the occurrence of SI after collision.

(4) Under the favorable conditions of collision-induced subduction transference, the time required for SI after collision is generally short within 10 Myrs, which is strongly dependent on the convergent boundary force, but weakly on the age of oceanic lithosphere.

(5) The SI of the Neo-Tethyan oceanic plate generally occurred shortly after the collision between the Cimmerian terranes and Eurasian continent, which may indicate the relatively large convergent force and/or weakened passive margin. In contrast, the stable Indian passive margin and absence of SI in the Indian Ocean may due to the low convergent force and/or the lack of proper weak zones, which still requires further studies.

Acknowledgment

The research leading to these results has received funding from the NSFC Tethys project (91855208), the Strategic Priority Research Program (B) of Chinese Academy of Sciences (XDB18000000), the NSFC normal project (41774108), as well as the support from the University of Chinese Academy of Sciences. Numerical simulations were run with the clusters of National Supercomputer Center in Guangzhou (Tianhe-II). *Taras Gerya*, *Di-Cheng Zhu*, and *Bo Wan* are acknowledged for the helpful discussion. The authors declare no conflict of interest. The figures of numerical models are produced by the Matlab of MathWorks and further compiled by the Adobe Illustrator. All related data will be provided in Zenodo (https://doi.org/xxxxx).

References

Aitchison, J. C., Ali, J. R., & Davis, A. M. (2007). When and where did India and Asia collide? Journal of Geophysical Research: Solid Earth, 112(B5).

Arcay, D., Lallemand, S., Abecassis, S., & Garel, F. (2019) Can subduction initiation at a transform fault be spontaneous? Solid Earth Discuss., https://doi.org/10.5194/se-2019-63, in review.

Arculus, R. J., Gurnis, M., Ishizuka, O., Reagan, M. K., Pearce, J. A., & Sutherland, R. (2019). HOW TO CREATE NEW SUBDUCTION ZONES. Oceanography, 32(1), 160-174.

Baes, M., Govers, R., & Wortel, R. (2011). Subduction initiation along the inherited weakness zone at the edge of a slab: Insights from numerical models. Geophysical Journal International, 184(3), 991-1008.

Baes, M., & Sobolev, S. V. (2017). Mantle flow as a trigger for subduction initiation: A missing element of the Wilson Cycle concept. Geochemistry, Geophysics, Geosystems, 18(12), 4469-4486.

Cloetingh, S., Wortel, R., & Vlaar, N. J. (1989). On the initiation of subduction zones. In Subduction Zones Part II (pp. 7-25). Birkhäuser Basel.

Crameri, F., Schmeling H., Golabek G. J., Duretz T., Orendt R., Buiter S., May D., Kaus B., Gerya T., & Tackley P. (2012), A comparison of numerical surface topography calculations in geodynamic modelling: an evaluation of the 'sticky air' method, Geophysical Journal International, 189, 38-54.

DeCelles, P. G., Kapp, P., Gehrels, G. E. & Ding L. (2014). Paleocene-Eocene foreland basin evolution in the Himalaya of southern Tibet and Nepal: Implications for the age of initial India-Asia collision. Tectonics 33, doi: 10.1002/2014TC003522.

Duretz, T., Gerya, T. V., Kaus, B. J. P., & Andersen, T. B. (2012). Thermomechanical modeling of slab eduction. Journal of Geophysical Research: Solid Earth, 117(B8).

Ghosh, A., Holt, W. E., Flesch, L. M., & Haines, A. J. (2006). Gravitational potential energy of the Tibetan Plateau and the forces driving the Indian plate. Geology, 34(5), 321-324.

Guilmette, C., Smit, M. A., van Hinsbergen, D. J., Gürer, D., Corfu, F., Charette, B., ... & Savard, D. (2018). Forced subduction initiation recorded in the sole and crust of the Semail Ophiolite of Oman. Nature Geoscience, 11(9), 688.

583 Gurnis, M., Hall, C. E., & Lavier, L. L. (2004), Evolving force balance during incipient subduction,
584 Geochemistry Geophysics Geosystems, 5(7).
585 Hall, R. (2018), The subduction initiation stage of the Wilson cycle, Geological Society, London, Special
586 Publications.
587 Harper, J. F. (1975). On the driving forces of plate tectonics. Royal Astronomical Society Geophysical Journal,
588 40, 465–474.0.
589 Karato, S., & Wu, P. (1993). Rheology of the upper mantle: A synthesis. Science, 260(5109), 771–778.
590 Kohn, M. & Parkinson, C. D. (2002). Petrologic case for Eocene slab breakoff during the Indo-Asian collision.
591 Geology 30, 591–594.
592 Leng, W., & Gurnis, M. (2011). Dynamics of subduction initiation with different evolutionary pathways.
593 Geochemistry, Geophysics, Geosystems, 12(12).
594 Li, Z.-H., Gerya, T., & Connolly, J. A. D. (2019). Variability of subducting slab morphologies in the mantle
595 transition zone: Insight from petrological-thermomechanical modeling. Earth-Science Reviews, 196,
596 102874.
597 Lippert, P. C., van Hinsbergen, D. J. J. & Dupont-Nivet, G. (2014). Early Cretaceous to present latitude of the
598 central proto-Tibetan Plateau: A paleomagnetic synthesis with implications for Cenozoic tectonics,
599 paleogeography, and climate of Asia. Geological Society of America Special Papers, 507, 1–21.
600 Mahatsente, R. (2017). Global models of ridge-push force, geoid, and lithospheric strength of oceanic plates.
601 Pure and Applied Geophysics, 174(12), 4395-4406.
602 Marques, F. O., Cabral, F. R., Gerya, T. V., Zhu, G., & May, D. A. (2014). Subduction initiates at straight
603 passive margins. Geology, 42(4), 331–334.
604 Marques, F. O., Nikolaeva, K., Assumpção, M., Gerya, T. V., Bezerra, F. H. R., do Nascimento, A. F., &
605 Ferreira, J. M. (2013). Testing the influence of far-field topographic forcing on subduction initiation at a
606 passive margin. Tectonophysics, 608, 517 - 524. https://doi.org/10.1016/j.tecto.2013.08.035
607 Mason, W. G., Moresi, L., Betts, P. G., & Miller, M. S. (2010). Three-dimensional numerical models of the
608 influence of a buoyant oceanic plateau on subduction zones. Tectonophysics, 483(1-2), 71-79.
609 Metcalfe, I. (2013). Gondwana dispersion and Asian accretion: Tectonic and palaeogeographic evolution of
610 eastern Tethys. Journal of Asian Earth Sciences, 66, 1-33.
611 Mueller, S., & Phillips, R. J. (1991). On the initiation of subduction. Journal of Geophysical Research: Solid
612 Earth, 96(B1), 651-665.
613 Müller, R. D., Sdrolias, M., Gaina, C., & Roest, W. R. (2008). Age, spreading rates and spreading symmetry of
614 the world's ocean crust. Geochemistry, Geophysics, Geosystems, 9, Q04006.
615 https://doi.org/10.1029/2007GC001743.
616 Najman, Y., Appel, E., Boudagherfadel, M. K., Bown, P. R., Carter, A., Garzanti, E., ... & Vezzoli, G. (2010).
617 Timing of India - Asia collision: Geological, biostratigraphic, and palaeomagnetic constraints. Journal of
618 Geophysical Research, 115, B12416, doi: 10.1029/2010JB007673.
619 Nikolaeva, K., Gerya, T. V., & Marques, F. O. (2011). Numerical analysis of subduction initiation risk along
620 the Atlantic American passive margins. Geology, 39(5), 463-466.
621 Niu, Y., O'Hara, M. J., & Pearce, J. A. (2003). Initiation of subduction zones as a consequence of lateral
622 compositional buoyancy contrast within the lithosphere: a petrological perspective. Journal of Petrology,
623 44(5), 851-866.
624 Pandey, D. K., Pandey, A., & Whattam, S. A. (2019). Relict subduction initiation along a passive margin in the
625 northwest Indian Ocean. Nature communications, 10(1), 2248.
626 Parlak, O., Dunkl, I., Karaoğlan, F., Kusky, T. M., Zhang, C., Wang, L., ... & Şimşek, G. (2019). Rapid
627 cooling history of a Neotethyan ophiolite: Evidence for contemporaneous subduction initiation and
628 metamorphic sole formation. Geological Society of America Bulletin.
629 Patriat, M., Falloon, T., Danyushevsky, L., Collot, J., Jean, M. M., Hoernle, K., ... & Feig, S. T. (2019).
630 Subduction initiation terranes exposed at the front of a 2 Ma volcanically-active subduction zone. Earth
631 and Planetary Science Letters, 508, 30-40.
632 Rey, P. F., Coltice, N., & Flament, N. (2014). Spreading continents kick-started plate tectonics. Nature,
633 513(7518), 405.
634 Searle, M. P. (2019). Timing of subduction initiation, arc formation, ophiolite obduction and India–Asia
635 collision in the Himalaya. Geological Society, London, Special Publications, 483(1), 19-37.

636 Selzer, C., Buiter, S. J., & Pfiffner, O. A. (2008). Numerical modeling of frontal and basal accretion at
637 collisional margins. Tectonics, 27(3).
638 Şengör, A. M. C., Altıner, D., Cin, A., Ustaömer, T., & Hsü, K. J. (1988). Origin and assembly of the
639 Tethyside orogenic collage at the expense of Gondwana Land. Geological Society, London, Special
640 Publications, 37(1), 119-181.
641 Shervais, J. W., Reagan, M., Haugen, E., Almeev, R. R., Pearce, J. A., Prytulak, J., ... & Li, H. (2019).
642 Magmatic Response to Subduction Initiation: Part 1. Fore - arc Basalts of the Izu - Bonin Arc From
643 IODP Expedition 352. Geochemistry, Geophysics, Geosystems, 20(1), 314-338.
644 Schmalholz, S. M., Medvedev, S., Lechmann, S. M., & Podladchikov, Y. (2014). Relationship between
645 tectonic overpressure, deviatoric stress, driving force, isostasy and gravitational potential energy.
646 Geophysical Journal International, 197(2), 680-696.
647 Schmeling, H., Babeyko, A. Y., Enns, A., Faccenna, C., Funiciello, F., Gerya, T., ... & Schmalholz, S. M.
648 (2008). A benchmark comparison of spontaneous subduction models—Towards a free surface. Physics of
649 the Earth and Planetary Interiors, 171(1-4), 198-223.
650 Stampfli, G. M., & Borel, G. D. (2002). A plate tectonic model for the Paleozoic and Mesozoic constrained by
651 dynamic plate boundaries and restored synthetic oceanic isochrons. Earth and Planetary Science Letters,
652 196(1-2), 17-33.
653 Stampfli, G. M., Hochard, C., Vérard, C., & Wilhem, C. (2013). The formation of Pangea. Tectonophysics,
654 593, 1-19.
655 Stern, R. J., & Gerya, T. V. (2018). Subduction initiation in nature and models: A review, Tectonophysics,
656 173-198.
657 Stern, R. J. (2017). Subduction initiation and terrane accretion, Geological Society of America Abstracts with
658 Program. Vol. 49, No. 6. doi: 10.1130/abs/2017AM-298141.
659 Stern, R. J., Reagan, M., Ishizuka, O., Ohara, Y., & Whattam, S. (2012). To understand subduction initiation,
660 study forearc crust: To understand forearc crust, study ophiolites. Lithosphere, 4(6), 469-483.
661 Stern, R. J. (2004). Subduction initiation: spontaneous and induced, Earth and Planetary Science Letters,
662 226(3), 275-292.
663 Sun, W. (2019). The Magma Engine and subduction initiation. Acta Geochimica, 38(5), 611-612.
664 https://doi.org/10.1007/s11631-019-00366-6
665 Tetreault, J. Á., & Buiter, S. J. H. (2012). Geodynamic models of terrane accretion: Testing the fate of island
666 arcs, oceanic plateaus, and continental fragments in subduction zones. Journal of Geophysical Research:
667 Solid Earth, 117(B8).
668 Turcotte D. L. & Schubert E. R. (1982). Geodynamics: Applications of continuum mechanics to geological
669 problems, Wiley, New York.
670 Turcotte, D.L., & Schubert G. (2002), Geodynamics, Cambridge University Press, Cambridge, UK.
671 Ulvrova, M. M., Coltice, N., Williams, S., & Tackley, P. J. (2019). Where does subduction initiate and cease?
672 A global scale perspective. Earth and Planetary Science Letters, 528, 115836.
673 van Hunen, J., van den Berg, A.P., & Vlaar, N.J., (2002). On the role of subducting oceanic plateaus in the
674 development of shallow flat subduction. Tectonophysics 352, 317–333.
675 van Hunen, J., van den Berg, A. P., & Vlaar, N. J. (2004). Various mechanisms to induce present-day shallow
676 flat subduction and implications for the younger Earth: a numerical parameter study. Physics of the Earth
677 and Planetary Interiors, 146(1-2), 179-194.
678 Vogt, K., & Gerya, T. V. (2014). From oceanic plateaus to allochthonous terranes: numerical modelling.
679 Gondwana Research, 25(2), 494-508.
680 Wan, B., Wu, F., Chen, L., Zhao, L., Liang, X., Xiao, W., & Zhu, R. (2019). Cyclical one-way continental
681 rupture-drift in the Tethyan evolution: Subduction-driven plate tectonics. Science China Earth Sciences,
682 1-12.
683 Wilmsen, M., Fürsich, F. T., Seyed-Emami, K., Majidifard, M. R., & Taheri, J. (2009). The Cimmerian
684 Orogeny in northern Iran: Tectono-stratigraphic evidence from the foreland. Terra Nova, 21(3), 211-218.
685 Yang, S. H., Li, Z.-H., Gerya, T., Xu, Z. Q., & Shi, Y. L. (2018). Dynamics of terrane accretion during
686 seaward continental drifting and oceanic subduction: Numerical modeling and implications for the
687 Jurassic crustal growth of the Lhasa Terrane, Tibet. Tectonophysics, 746, 212-228.

Yin, A., & Harrison, T. M. (2000). Geologic evolution of the Himalayan-Tibetan orogen. Annual review of earth and planetary sciences, 28(1), 211-280.

Zanchi A, Zanchetta S, Balini M, & Ghassemi M R. (2016). Oblique convergence during the Cimmerian collision: Evidence from the Triassic Aghdarband Basin, NE Iran. Gondwana Research, 38: 149–170.

Zhong, X., & Li, Z.-H. (2019). Forced subduction initiation at passive continental margins: Velocity - driven v ersus stress-driven. Geophysical Research Letters, 46, 11,054–11,064. https://doi.org/10.1029/2019GL08 4022.

Zhou, X., Li, Z. H., Gerya, T. V., Stern, R. J., Xu, Z., & Zhang, J. (2018). Subduction initiation dynamics along a transform fault control trench curvature and ophiolite ages. Geology, 46(7), 607–610.

Zhu, D.C., Mo, X.X., Niu, Y.L., Zhao, Z.D., Wang, L.Q., Liu, Y.S., & Wu, F.Y. (2009). Geochemical investigation of Early Cretaceous igneous rocks along an east−west traverse throughout the central Lhasa Terrane, Tibet. Chemical Geology 268, 298–312.

Zhu, D. C., Zhao, Z. D., Niu, Y., Mo, X. X., Chung, S. L., Hou, Z. Q., ... & Wu, F. Y. (2011). The Lhasa Terrane: record of a microcontinent and its histories of drift and growth. Earth and Planetary Science Letters, 301(1-2), 241-255.

Zhu, D. C., Zhao, Z. D., Niu, Y., Dilek, Y., Hou, Z. Q., & Mo, X. X. (2013). The origin and pre-Cenozoic evolution of the Tibetan Plateau. Gondwana Research, 23(4), 1429-1454.

Zhu, D. C., Wang, Q., Zhao, Z. D., Chung, S. L., Cawood, P. A., Niu, Y., ... & Mo, X. X. (2015). Magmatic record of India-Asia collision. Scientific Reports, 5, 14289.

References in Supporting Information

Bina, C. R., & Helffrich, G. (1994). Phase transition Clapeyron slopes and transition zone seismic discontinuity topography. Journal of Geophysical Research: Solid Earth, 99(B8), 15853-15860.

Bittner, D., & Schmeling, H. (1995). Numerical modelling of melting processes and induced diapirism in the lower crust. Geophysical Journal International, 123(1), 59-70.

Clauser, C., & Huenges, E. (1995). Thermal conductivity of rocks and minerals. Rock physics and phase relations: a handbook of physical constants, 3, 105-126.

Connolly, J. A. (2005). Computation of phase equilibria by linear programming: a tool for geodynamic modeling and its application to subduction zone decarbonation. Earth and Planetary Science Letters, 236(1-2), 524-541.

Connolly, J. A. D. (2009). The geodynamic equation of state: what and how. Geochemistry, Geophysics, Geosystems, 10(10).

Dziewonski, A. M., & Anderson, D. L. (1981). Preliminary reference Earth model. Physics of the earth and planetary interiors, 25(4), 297-356.

Gerya, T.V. (2010). Introduction to numerical geodynamic modelling, Cambridge University Press, Cambridge, UK.

Gerya, T. V., & Meilick, F. I. (2011). Geodynamic regimes of subduction under an active margin: effects of rheological weakening by fluids and melts. Journal of Metamorphic Geology, 29(1), 7-31.

Gorczyk, W., Willner, A. P., Gerya, T. V., Connolly, J. A., & Burg, J. P. (2007). Physical controls of magmatic productivity at Pacific-type convergent margins: Numerical modelling. Physics of the Earth and Planetary Interiors, 163(1-4), 209-232.

Ito, K., & Kennedy G. (1971). An experimental study of the basalt-garnet granulite-eclogite transition, in: Heacock J.G. (eds.), The Structure and Physical Properties of the Earth's Crust, Geophysical Monograph Series, 14, 303-314, AGU, Washington D.C., USA.

Ito, E., & Takahashi, E. (1989). Postspinel transformations in the system Mg_2SiO_4 - Fe_2SiO_4 and some geophysical implications. Journal of Geophysical Research: Solid Earth, 94(B8), 10637-10646.

Ito, E., Akaogi M., Topor L., & Navrotsky A. (1990). Negative pressure-temperature slopes for reactions forming $MgSiO_3$ perovskite from calorimetry, Science, 249, 1275-1278.

737 Ito, K., & Kennedy G. (2013). An experimental study of the basalt-garnet granulite-eclogite transition, in:
738 Heacock, J.G. (Ed.), The Structure and Physical Properties of the Earth's Crust, American Geophysical
739 Union, Washington, DC.
740 Kameyama, M., Yuen, D. A., & Karato, S. I. (1999). Thermal-mechanical effects of low-temperature plasticity
741 (the Peierls mechanism) on the deformation of a viscoelastic shear zone. Earth and Planetary Science
742 Letters, 168(1-2), 159-172.
743 Karato, S., Riedel M., & Yuen D.A. (2001). Rheological structure and deformation of subducted slabs in the
744 mantle transition zone: Implications for mantle circulation and deep earthquakes. Physics of the Earth and
745 Planetary Interiors, 127, 83-108.
746 Katsura, T., & Ito E. (1989). The System Mg_2SiO_4-Fe_2SiO_4 at High Pressures and Temperatures: Precise
747 Determination of Stabilities of Olivine, Modified Spinel, and Spinel, Journal of Geophysical Research:
748 Solid Earth, 94(B11), 15663-15670.
749 Katz, R.F., Spiegelman M., & Langmuir C.H. (2003). A new parameterisation of hydrous mantle melting,
750 Geochemistry, Geophysics, Geosystems, 4, 1073.
751 Kirby, S.H., & Kronenberg A.K. (1987). Rheology of the lithosphere: selected topics, Reviews of Geophysics,
752 25, 1219-1244.
753 Li, Z.-H., Liu M., & Gerya T. (2016). Lithosphere delamination in continental collisional orogens: A
754 systematic numerical study, Journal of Geophysical Research: Solid Earth, 121, 5186-5211.
755 Peacock S.M. (1990), Fluid processes in subduction zones, Science, 248, 329-337.
756 Ranalli, G. (1995). Rheology of the earth, deformation and flow process in geophysics and geodynamics (2nd
757 ed.), Chapman & Hall, London, UK.
758 Rubie, D. C., & Ross II, C. R. (1994). Kinetics of the olivine-spinel transformation in subducting lithosphere:
759 Experimental constraints and implications for deep slab processes. Physics of the Earth and Planetary
760 Interiors, 86(1-3), 223-243.
761 Schmidt, M. W., & Poli, S. (1998). Experimentally based water budgets for dehydrating slabs and
762 consequences for arc magma generation. Earth and Planetary Science Letters, 163(1-4), 361-379.
763